TITLE: A Proteomic Atlas of Senescence-Associated Secretomes for Aging Biomarker Development

Authors: Nathan Basisty[1], Abhijit Kale[1], Okhee Jeon[1], Chisaka Kuehnemann[1], Therese Payne[1], Chirag Rao[1], Anja Holtz[1], Samah Shah[1], Luigi Ferrucci[3], Judith Campisi[1, 2], Birgit Schilling**[1]

[1] The Buck Institute for Research on Aging, Novato, California 94947, USA.

[2] Lawrence Berkeley Laboratory, University of California, Berkeley, California 94720, USA.

[3] National Institute on Aging, Bethesda, Maryland 20892, USA.

** Correspondence: bschilling@buckinstitute.org

SUMMARY: The senescence-associated secretory phenotype (SASP) has recently emerged as both a driver of, and promising therapeutic target for, multiple age-related conditions, ranging from neurodegeneration to cancer. The complexity of the SASP, typically monitored by a few dozen secreted proteins, has been greatly underappreciated, and a small set of factors cannot explain the diverse phenotypes it produces *in vivo*. Here, we present 'SASP Atlas', a comprehensive proteomic database of soluble and exosome SASP factors originating from multiple senescence inducers and cell types. Each profile consists of hundreds of largely distinct proteins, but also includes a subset of proteins elevated in all SASPs. Based on our analyses, we propose several candidate biomarkers of cellular senescence, including GDF15, STC1 and SERPINs. This resource will facilitate identification of proteins that drive specific senescence-associated phenotypes and catalog potential senescence biomarkers to assess the burden, originating stimulus and tissue of senescent cells *in vivo*.

INTRODUCTION:

Cellular senescence is a complex stress response that causes an essentially irreversible arrest of cell proliferation and development of a multi-component senescence-associated secretory phenotype (SASP) (Acosta et al., 2008; Coppé et al., 2008, 2010a; Kuilman et al., 2008). The SASP consists of myriad cytokines, chemokines, growth factors, and proteases that initiate inflammation, wound healing, and growth responses in nearby cells and tissues (Neves et al., 2015; Tchkonia et al., 2013). In young and healthy tissues, the SASP is typically transient and tends to contribute to the preservation or restoration of tissue homeostasis (Neves et al., 2015). However, the increase in senescent cells with age and a chronic SASP are now known to be key drivers of many pathological hallmarks of aging, including chronic inflammation, tumorigenesis, impaired stem cell renewal, and others (Neves et al., 2015; Tominaga, 2015). Using either or both of two transgenic mouse models that allow the selective elimination of senescent cells (Baker et al., 2011; Demaria et al., 2014), or compounds that mimic the effect of these transgenes, data from several laboratories strongly support the idea that the presence of senescent cells drives multiple age-related phenotypes and pathologies, including age-related atherosclerosis (Childs et al., 2016), osteoarthritis (Jeon et al., 2018), cancer metastasis and cardiac dysfunction (Baar et al., 2017; Demaria et al., 2017), myeloid skewing in the bone marrow (Abdul-Aziz et al., 2018; Chang et al., 2016), kidney dysfunction (Valentijn et al., 2018), and overall decrements in healthspan (Baker et al., 2016).

Several types of stress elicit a senescence and secretory response, which in turn can drive multiple phenotypes and pathologies associated with aging in mammals. Some of these stressors have shared effects. For example, telomere attrition resulting from repeated cell division (replicative senescence), elevated reactive oxygen species, chromatin disruption, and even the activation of certain oncogenes all can cause genotoxic stress, as can a number of therapeutic drug treatments, such as anti-cancer chemotherapies (Demaria et al., 2017) and certain highly active antiretroviral therapies for HIV treatment or prevention (Hernandez-Vallejo et al., 2013). However, whether these stressors produce similar or distinct SASPs is at present poorly characterized. Therefore, a comprehensive characterization of SASP components is critical to

understanding how senescent response can drive such diverse pathological phenotypes *in vivo*. It is also a critical step in clarifying how various stimuli, all acting through senescence, differentially affect health.

The SASP was originally characterized by antibody arrays, which are necessarily biased, to measure the secretion of a small set of pro-inflammatory cytokines, proteases and protease inhibitors, and growth factors (Acosta et al., 2008; Coppé et al., 2008; Kuilman et al., 2008; Rodier et al., 2009). Subsequently, numerous large-scale unbiased gene expression studies were performed on different tissues and donors of varying ages, all of which indicated the existence of a complex and robust secretory program in senescent cells (Coppé et al., 2010b). A recent meta-analysis of senescent cell transcriptomes confirmed the expression of a few dozen of the originally characterized SASP factors in multiple senescent cell types (Hernandez-Segura et al., 2017). While unbiased comprehensive genomic analyses are valuable in describing the overall phenotype of senescent cells, the transcriptome only modestly correlates with the proteome, and cannot accurately and quantitatively assess the *secreted* protein profiles. Thus, transcriptomic profiles are unlikely to identify novel SASP factors without protein verification. Recently, the SASP induced by several genotoxic stressors was qualitatively assessed using mass spectrometry-based proteomics (Özcan et al., 2016). However, an in-depth, quantitative assessment of the SASP originating from multiple stimuli and cell types is missing. In addition, the secretion of exosomes and their contents by senescent cells has also been recently reported (Takasugi, 2018). Others have investigated the miRNA components of senescent exosomes but, aside from pro-tumorigenic effects (Takasugi, 2018), the proteomic content and function of exosomes and small extracellular vesicles (EVs) secreted by senescent cells remains largely unknown.

Studies of the SASP have made it clear that the SASP is not a single phenotype, but a series of highly complex and dynamic phenotypes that vary depending on the inducer of senescence and cell type. Given the growing size and complexity of the SASP, a central resource is needed for researchers to reference and more precisely interrogate context-dependent senescent phenotypes. Here we present “SASP Atlas” (www.SASPAtlas.com), a comprehensive, curated and expanding online database of

the soluble secretomes of senescent cells (sSASPs) induced by various stimuli and in several cell types. We also present the first comprehensive proteomic analysis of the exosomal SASP (eSASP), which is largely distinct from the sSASP. Our proteomic analysis leverages a modern data-independent acquisition (DIA or SWATH) mass spectrometry workflow, which comprehensively acquires label-free, quantitative peptide (MS1) and fragment-level (MS2) data for all peptides in each sample (Bruderer et al., 2015; Egertson et al., 2015; Gillet et al., 2012; Rardin et al., 2015; Schilling et al., 2017). DIA workflows are not limited by stochastic peptide MS/MS sampling biases introduced by more traditional data-dependent acquisition (DDA) mass spectrometry. In addition to our interactive, online database (SASP Atlas), we assembled and deposited proteomic panels of SASP factors on Panorama Web, a freely-available web-repository for targeted mass spectrometry assays (Sharma et al., 2014, 2018) as a resource for others to detect and quantify the SASP in mass spectrometric studies.

The physiological effects of senescent cells derive largely from their ability to alter the behavior and function of neighboring cells through the secretion of proteins and other bioactive molecules, both locally within the tissue of residence and systemically throughout the organism. Comprehensive characterization of the SASPs originating from multiple stresses and cell types will help identify biomarkers associated with a number of diseases driven by the presence of senescent cells. Inhibiting the SASP or selectively removing senescent cells is a promising strategy to combat many age-related diseases and improve healthspan (Baker et al., 2016), and has driven efforts to develop drugs, such as senolytics and SASP inhibitors, for use in humans.

RESULTS AND DISCUSSION:

Cellular senescence drives robust and variable changes in the secreted proteome

The secretomes of senescent cells and quiescent control cells were obtained from cultured primary human lung fibroblasts (IMR90) and renal cortical epithelial cells, as shown in **Figure 1**. Briefly, senescence was induced in cultured cells by one of three senescence-inducing stimuli: X-ray irradiation (IR), inducible RAS overexpression (RAS), or treatment with the protease inhibitor atazanavir (ATV). Secreted soluble proteins and exosomes/EVs were obtained from the conditioned media of senescent

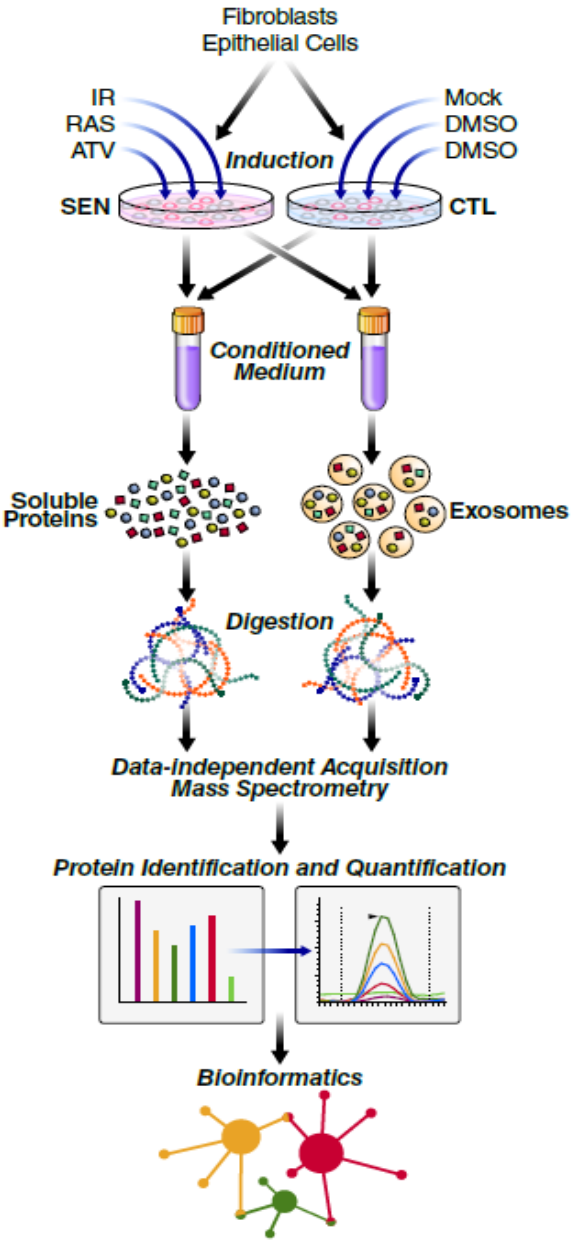

Figure 1. Proteomic workflow for isolation and analysis of secreted proteins & exosomes/EVs. Senescence was induced in cultured primary human lung fibroblasts and renal epithelial cells by one of three stimuli: X-ray irradiation (IR), inducible RAS overexpression (RAS), or treatment with atazanavir (ATV), and cultured for 10 days, 7 days, or 14 days for IR, RAS, and ATV, respectively. In parallel, control cells were made quiescent by incubation in 0.2% serum for 3 days and were either mock- or vehicle- treated. Following development of senescence, treated and control cells were cultured in serum-free medium for 24 hours and conditioned medium was collected. Secreted soluble proteins and exosomes/EVs from each sample were separated by ultracentrifugation. All protein samples were digested and subjected to data-independent acquisition (DIA), followed by protein identification and quantification using Spectronaut Pulsar (Biognosys, Bruderer et al., 2015) and by Bioinformatic, pathway and network analysis in R and Cytoscape (Bindea et al., 2009; Shannon et al., 2003). SEN = Senescent, CTL = Control,

and control cells. Protein identification and quantification was then performed using a label-free, comprehensive and unbiased data-independent acquisition (DIA) approach, which enables more sensitive and accurate quantification of proteins by integration of MS2 fragment ion chromatograms. For quantification of relative abundances, proteins secreted by senescent cells were compared with their respective controls, and significantly changed proteins (q-value <0.05) were identified. Proteins secreted at higher levels by senescent, relative to quiescent, cells were defined as SASP components. Most SASP components were secreted at very high levels by senescent cells versus non-senescent cells (**Figure 2**). Each treatment group and respective controls contained between 4 and 10 biological replicates (see STAR Methods for replicate details). Relative protein quantification and statistical details for all secretomes are presented in **Table S1**. Induction of senescence

was independently validated by measuring senescence-associated β-galactosidase (SA-β-Gal) staining and p16INK4a and IL-6 mRNA levels (**Figure S1**), as described (Coppé et al., 2008). There was no detectable cell death, as measured by a Sytox Green viability dye assay (**Figure S2**). X-irradiation and RAS overexpression induced senescence in >90% of cells and ATV induced senescence in about 65% of cells, as measured by SA-β-Gal staining (**Figure S1A-B**).

This unbiased proteomic profiling identified up to ~1700 secreted proteins, a large fraction of which were up- or down-regulated following induction of senescence by IR, RAS, or ATV (**Figure 2**), ranging between 376 to 747 significant changes per inducer. As expected, most of the significantly changed secreted proteins were markedly upregulated in senescent, compared to quiescent, cells, but interestingly, a minority were downregulated (**Figure 2A**). Notably, the protein cargo of exosomes/EVs released by senescent cells was substantially distinct compared to non-senescent cells

A

	Secretome (Soluble)	Exosomes
IR Geno-toxic	1505 Proteins **554**↑ (531 >2-fold Increase) **38**↓ (32 >2-fold Decrease)	1502 Proteins **144**↑ (111 >2-fold Increase) **326**↓ (221 >2-fold Decrease)
RAS Onco-genic	1693 Proteins **730**↑ (675 >2-fold Increase) **17**↓ (10 >2-fold Decrease)	354 Proteins **22**↑ (19 >2-fold Increase) **20**↓ (14 >2-fold Decrease)
ATV Treat-ment	441 Proteins **362**↑ (271 >2-fold Increase) **14**↓ (7 >2-fold Decrease)	

B

Cell Type	
Fibro	1505 Proteins **554**↑ (531 >2-fold Increase) **38**↓ (32 >2-fold Decrease)
Epi	1181 Proteins **489**↑ (73 >2-fold Increase) **341**↓ (64 >2-fold Decrease)

C

		Proteins							RNA		Activity
		CXCL1	CXCL8	HMGB1	IGFBP: 2|3|4|5|7	MMP1 MMP2	LAMB1	TIMP1 TIMP2	p16	IL-6	SA-β-Gal
Fibro	IR	↑	↑	↑	↑↑↑↑↑	↑↑	↑	↑↑	↑	↑	↑
	RAS	↑	↑	↑	↑↑↑↑↑	↑↑	↑	↑↑	↑	↑	↑
	ATV	↑	–	↑	↑↑↑↑↑	↑↑	↑	↑↑	↑	↑	↑
Epi	IR	↓	–	–	↑–↓–↓	––	↓	↓↓	↑	↑	↑
Exo-some	IR	–	–	↑	–↓↓↓↓	–↓	↓	↓↓			
	RAS	–	–	–	––↑––	––	–	–			

Figure 2. Proteomic profiling of the soluble and exosome/EV SASP following induction of senescence by various stimuli. A) Summary of proteins with significantly altered (q-value<0.05) secretion in senescent cells versus quiescent controls following genotoxic-stress, oncogenic stress, and treatment stress. B) Significantly altered levels of protein secreted by senescent lung fibroblasts and renal epithelial cells compared with quiescent control cells. C) The presence of commonly reported SASP markers in each inducer, cell type, and fraction. IR = X-irradiation, RAS = RAS oncogene overexpression, ATV = atazanavir treatment, Fibro = fibroblasts, Epi = renal epithelial cells.

(**Figure 2A**), indicating the existence of an exosome/EV SASP (eSASP) in addition to the sSASP.

The majority of changes in the sSASP, independent of inducer, exhibited increased secretion by senescent cells, with only 2-6% of proteins secreted at lower levels. In contrast, one-half to two-thirds of all significant protein changes in exosomes/EVs from senescent fibroblasts were decreased relative to quiescent cells (**Figure 2A**). For senescent renal epithelial cells, the sSASP comprised a more even mix of proteins with significantly lower or higher relative secretion. While the renal epithelial cell sSASP contained more overall changes than the fibroblast sSASP (830 versus 592 significant protein changes following IR), the magnitude of the fold-changes in the sSASP were higher in fibroblasts regardless of inducer (**Figure 2B**). For example, 95% of significant changes in the fibroblast sSASP were >2-fold, compared to only 17% of changes in the renal epithelial cell sSASP.

For each cell type and fraction, we checked for previously identified markers of senescence and the SASP (**Figure 2C**). These markers included chemokines (CXCLs), high mobility group box 1 protein (HMGB1), IGF binding proteins (IGFBPs), matrix metalloproteinases (MMPs), lamin b1 (LMNB1), and tissue inhibitors of metallopeptidase (TIMPs). In addition, we measured mRNA levels of p16INK4a (CDKN2A) and interleukin-6 (IL-6), and SA-β-Gal staining (**Figure S1C**). In fibroblasts, all previously identified senescence and SASP markers were elevated, regardless of the senescence inducer. However, while expression of p16INK4a, IL-6 and SA-β-Gal were also elevated in renal epithelial cells, the proteins secreted by fibroblasts were either decreased or unchanged, except for IGFBP2. This finding suggests that fibroblast SASP markers are not sufficient to detect senescence and that profiling the SASP in different cell types and biological contexts is required to detect senescent cells *in vivo* with confidence. Within exosomes/EVs secreted by senescent fibroblasts, nearly all previously identified SASP factors were either absent, unchanged or decreased, and none were consistently elevated in response to more than one inducer (**Figure 2C**).

Senescence-inducing stresses drive largely distinct secretory phenotypes

To determine the effect of senescence-inducing stimuli on the SASPs of senescent cells, we compared the sSASP from human primary fibroblasts induced to senesce by IR, RAS or ATV. Strikingly, the sSASP was largely distinct among inducers, with an overlap of 172 proteins among 1107 total increased proteins and no overlap among decreased proteins (**Table S2**). Thus, most protein changes were not shared among inducers (**Figure 3A**). Among the overlapping increased proteins, levels varied among inducers (**Figure 3B**). In particular, the ATV-induced sSASP had fewer and generally smaller changes than either the RAS- or IR-induced sSASP, perhaps corresponding to less efficient induction of senescence, as determined by SA-β-Gal staining (**Figure S1**).

To determine whether there is a core of pathways or functions associated with the SASPs, we performed pathway and network analysis on proteins that overlapped in the sSASPs of each inducer (**Figure 3C**). The largest pathway networks associated with all inducers related to tissue and cell structure and organization, including extracellular matrix, cytoskeleton, integrins, and peptidase activity. Interestingly, neurodegeneration and three related pathways with high agreement (kappa score >40%) – apoptosis, ROS signaling and TP53-regulated metabolism - were also enriched among overlapping sSASP proteins (**Figure 3C-D**). Among the neurodegeneration proteins were amyloid precursor protein (APP) and cystatin 3 (CST3), related to Alzheimer's pathogenesis and risk (Kaur and Levy, 2012; O'Brien and Wong, 2011), as well as Parkinsonism-associated deglycase (PARK7 or DJ1) (Bonifati et al., 2003) (**Figure 3D**). This enrichment of neurodegeneration-associated proteins and highly connected pathways suggests that senescence may contribute to pathogenesis of neurodegenerative diseases, for which these sSASP factors might serve as biomarkers, regardless of the senescence-inducing stimuli. Further research will be needed to assess the value of these proteins as biomarkers.

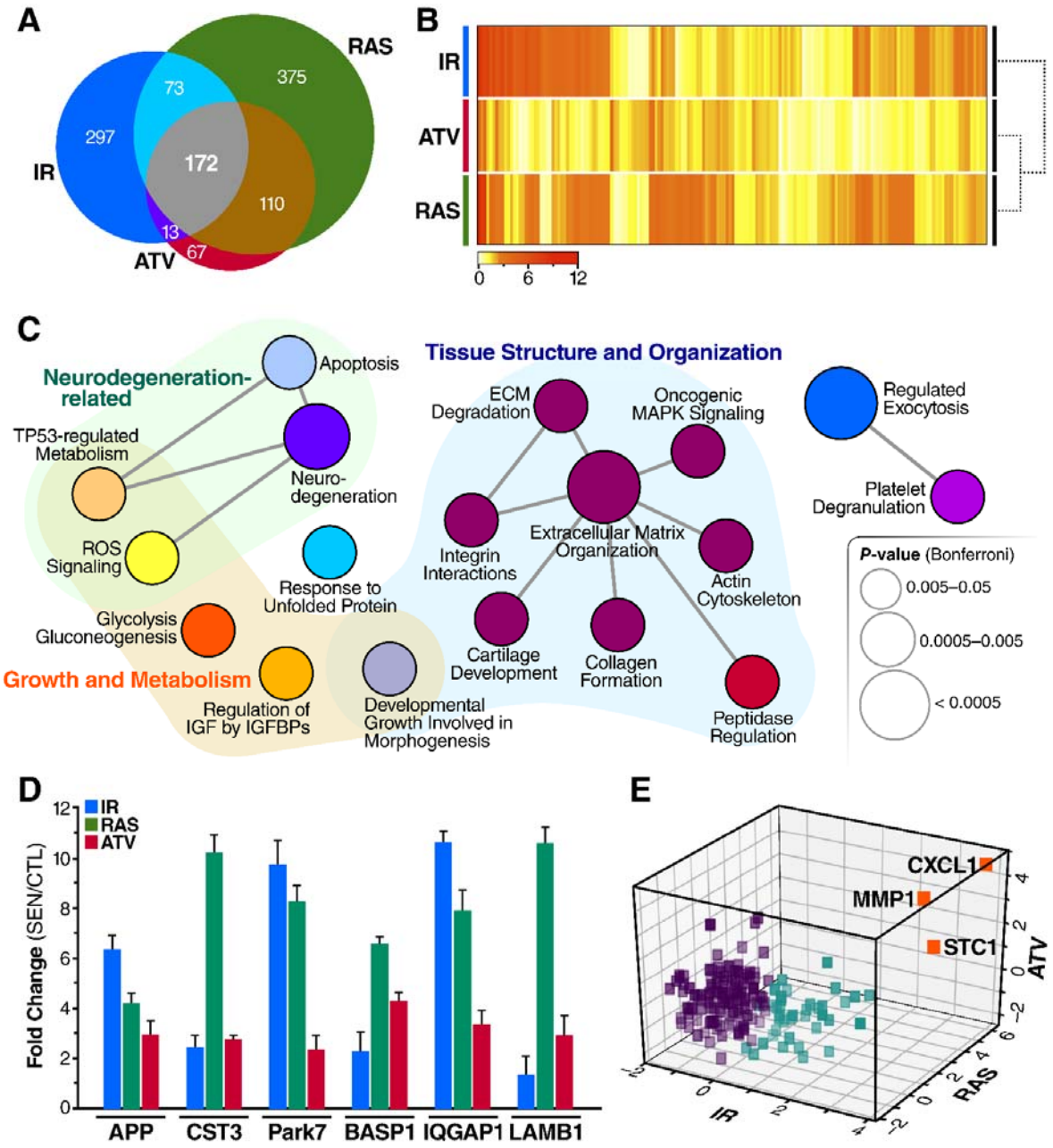

Figure 3. Core sSASP proteins, networks and pathways. A) Venn diagram of proteins with significantly increased secretion in senescent versus non-senescent fibroblasts following induction of senescence by IR, RAS or ATV. B) Heatmap of significantly increased (q-value < 0.05) sSASP factors common to each senescence-inducing stimuli. C) ClueGO (Bindea et al., 2009) pathway enrichment and network analysis of overlapping sSASPs from each senescence inducer. Pathways of the same color have >= 50% similarity in terms. Edges represent Kappa connectivity scores >40%. D) Secretion levels of proteins in the neurodegeneration pathway in IR-, RAS- and ATV-induced senescent cells, expressed as log2 fold change of senescent versus control. E) K-means clustering of proteins significantly increased in the sSASP of all inducers. The protein values, which are log2 fold changes of senescence versus control, were used to partition the data into 3 clusters. IR = X-irradiation, RAS = RAS oncogene overexpression, ATV = atazanavir treatment.

To distill the overlapping 'core' sSASP proteins into primary components in an unbiased fashion, we performed an unsupervised machine learning analysis on the levels of secreted proteins (**Figure 3E**). K-means clustering analysis uncovered three primary clusters among core sSASP components. Strikingly, one cluster consisting of just three proteins – chemokine (C-X-C motif) ligand 1 (CXCL1), matrix metallopeptidase 1 (MMP1), and stanniocalcin 1 (STC1) – were very highly present in the sSASP of all inducers, suggesting that these proteins are best qualified to serve as surrogate markers of the sSASP. Of note, among the top expressed sSASP proteins was STC1, a previously unidentified SASP factor and a secreted hormone with many disease associations (Chang et al., 2015; Du et al., 2016; Ohkouchi et al., 2015; Pan et al., 2015; Shahim et al., 2017; Su et al., 2015), demonstrating the utility of robust unbiased approaches to uncovering novel molecules, biological functions and pathways. Our approach also validates MMP1 and CXCL1 as SASP markers.

The sSASP is largely distinct in composition and regulation in fibroblasts and epithelial cells

We also compared the secretomes of fibroblasts and renal epithelial cells to understand the cell-type specificity of the sSASP. Indeed, the sSASP of fibroblasts and epithelial cells were largely distinct (**Figure 4A-B**). Among the proteins increased in the sSASP of each cell type, 20-30% overlapped, and the magnitude of the change by renal epithelial cells was, in most cases, lower than in fibroblasts, although it is possible that senescent fibroblasts inherently secrete more proteins than epithelial cells. Senescent epithelial cells also secreted significantly lower levels of many proteins, compared to senescent fibroblasts, regardless of senescence inducer. Interestingly, 20-30% of the proteins significantly decreased in the sSASP of renal epithelial cells overlapped with proteins significantly increased in the fibroblast sSASP (**Figure 4B**), suggesting a negative correlation of a portion of the sSASP between cell types. Among the epithelial sSASP factors that changed oppositely to fibroblast sSASP factors were IGFBPs, TIMPs 1 and 2, CXCL1, and most SERPINs (**Figure 2C**). In all, 54 sSASP factors were shared between all senescence inducers and cell types that we examined (**Table S3**).

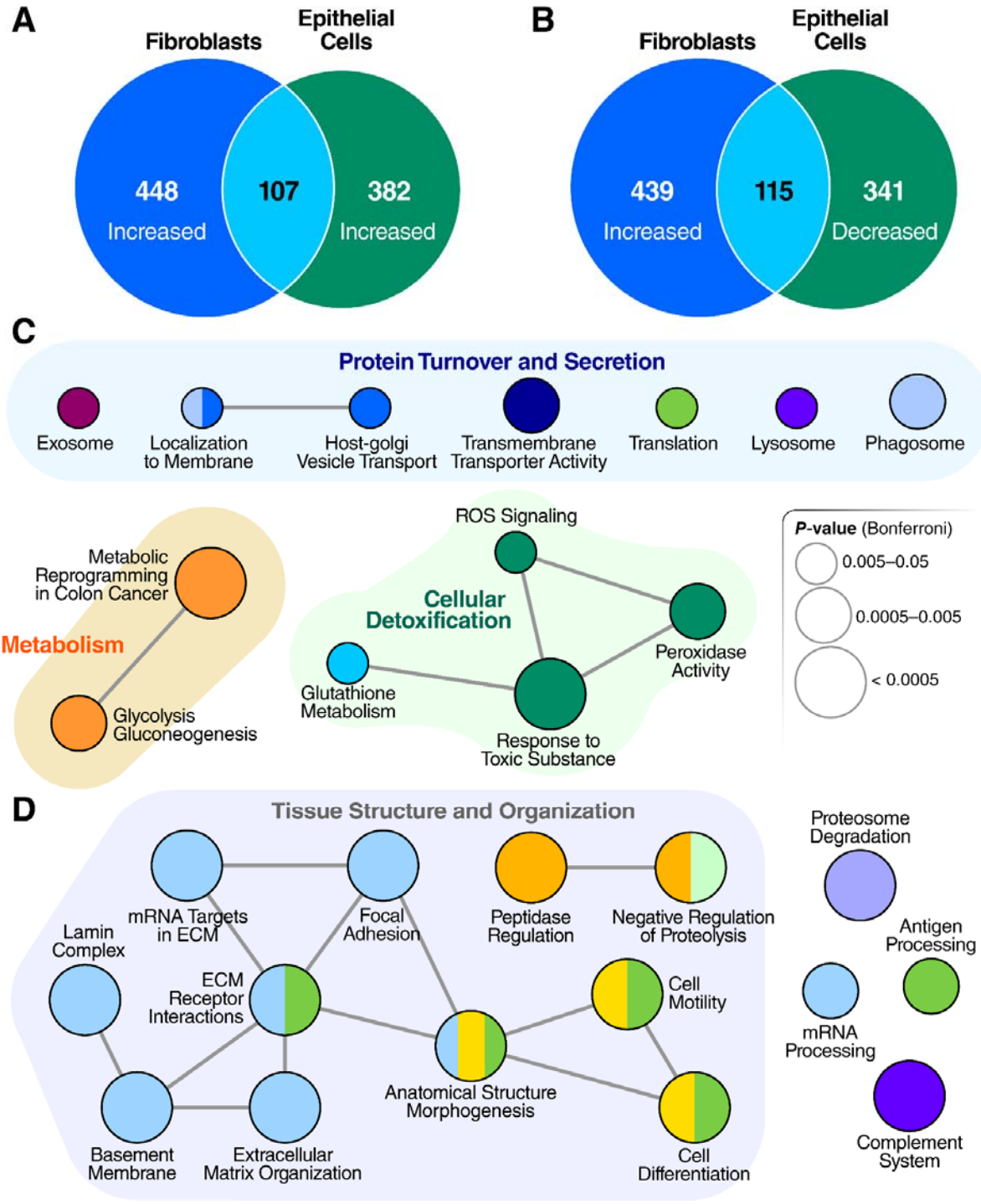

Figure 4. Renal epithelial cells and fibroblasts express distinct sSASPs. A) Venn diagram comparing proteins increased in the sSASP of senescent fibroblasts vs senescent epithelial cells induced by X-irradiation. B) Venn diagram comparing protein increases in the fibroblast sSASP vs *decreases* in the epithelial sSASP. C) Pathway and network analysis of proteins highly secreted by senescent fibroblasts and epithelial cells. C) Pathway and network analysis of proteins significantly increased in the fibroblast sSASP but significantly decreased in the epithelial cell sSASP.

Pathway and network analysis of proteins increased in the sSASPs of fibroblasts and epithelial cells (**Figure 4C**) showed that most pathways belonged to one of three general categories: protein turnover and secretion, primary metabolism, and cellular detoxification. While not as apparent on a molecule-by-molecule basis, on the pathway level many functions were commonly enriched in both the epithelial and fibroblast sSASPs (**Figure 4C** and **Figure 3C**), including vesicle-mediated transport and exosomes, glycolytic metabolism, and cellular detoxification. The notable exceptions enriched uniquely by epithelial cells are protein translation and degradation (lysosome and phagosome).

Surprisingly, the majority of renal epithelial sSASP proteins with significantly lower secretion were enriched in pathways related to tissue and cell structure, adhesion and motility (**Figure 4D**). This is in contrast to previous reports and our own findings in fibroblasts (**Figure 3C**), in which these functions were most highly increased, regardless of inducer. The irradiated epithelial sSASP also had significantly lower levels of proteins involved in RNA processing, in contrast to increased RNA metabolism in the irradiated fibroblast sSASP. Additionally, the epithelial sSASP was significantly depleted in proteins related to proteasome degradation, antigen processing, and the complement system.

Damage-associated molecular patterns (DAMPs, also known as alarmins or danger signals) are released from cells in response to internal and external stressors, and have been identified as components of the SASP (Davalos et al., 2013). Pattern recognition receptor-bearing cells, including cells of the innate immune system, recognize extracellular DAMPs as signals to promote inflammatory and fibrotic responses in tissues. An increase in circulating DAMPs is hypothesized to play a role in aging (Feldman et al., 2015; Huang et al., 2015), particularly in the age-related inflammation termed ‘inflammaging’ (Franceschi and Campisi, 2014). DAMPs may also be biomarkers of a number of diseases, including traumatic, cardiovascular, metabolic, neurodegenerative, malignant, and infectious diseases (Feldman et al., 2015; Fucikova et al., 2015; Garg et al., 2015). HMGB1, a founding member of the DAMPs, is a prominent SASP marker (Davalos et al., 2013). Our proteomic analysis identified increased secretion of multiple DAMPs, including the prototypical molecules HMGB1

and calreticulin (CALR), by senescent fibroblasts under all senescence-inducing stresses (**Table 1**). However, in senescent epithelial cells the secretion of DAMPs was either unchanged or significantly reduced, demonstrating that some defining SASP components may vary depending on cell type.

	Log2(SEN/CTL)			
	IR (Fibroblasts)	**RAS**	**ATV**	**IR (Epithelial)**
HMGB1	2.47	0.59	2.46	NS
CALR	1.22	0.51	1.32	-1.00
CD44	2.25	1.20	1.92	-0.69
S100A11	0.56	1.35	1.88	NS
LGALS3BP	1.46	1.76	1.79	-1.19
VCAN	1.80	1.32	0.98	-1.42
TNC	1.64	1.40	2.46	0.29
HSPA5	2.03	3.93	1.78	-0.34
HSP90AB1	5.01	2.69	1.65	NS
HSPA8	2.49	2.98	1.46	0.32
HSPA1A	2.96	2.4	1.45	0.54
HSP90AA1	4.94	3.42	1.34	NS
HSP90B1	2.67	1.61	0.66	-0.27

Table 1: DAMPs are a core component of the fibroblast SASP. SEN = Senescent, CTL = Control, IR = X-irradiation, RAS = RAS overexpression, ATV = Atazanavir treatment.

Exosome/EV characteristics and proteomic contents are altered by cellular senescence.

Because exosome and vesicle-mediated transport proteins are enriched in the soluble SASP, we hypothesized that senescent cells would show significant changes in exosome biology and proteomic content, or the exosome/EV SASP (eSASP). We used an ultracentrifugation-based protocol to enrich conditioned media for exosomes and small EVs released by quiescent and senescent fibroblasts induced by X-irradiation and RAS overexpression (**Figure 1**, see methods). We confirmed the presence of exosome/EV markers, such as CD63 and CD9 (Keerthikumar et al., 2016), in the purified fractions and the absence of exosome/EV markers in EV-depleted soluble fractions (**Figure S3A**). Exosomes/EVs from senescent fibroblasts had a robustly altered proteomic composition compared with exosomes from non-senescent cells (**Figure 2A**).

To determine whether the secretion and characteristics of exosomes/EVs are altered in senescent cells, we performed particle counting and size distribution analysis of exosomes/EVs secreted into the culture medium of senescent and non-senescent cells over a 24-hour period. On average, senescent cells released a smaller number of vesicles -- about 275 vesicles per cell compared to 374 vesicles per cell in controls (**Figure 5A**). However, the mean diameter, size distribution and protein content of senescent exosomes/EVs was significantly greater than controls (**Figure 5B-C, Figure S3B-C**). Of note, a recent study examining EVs in humans reported a decline in the concentration and increase in size of EVs circulating in the plasma of older, compared to younger, individuals (Eitan et al., 2017). These findings are consistent with an expected increase in senescent cell burden with age. Further work with senolytics may validate whether exosome/EV concentration and size are indicators of senescent cell burdens in humans.

The protein content of exosomes/EVs released by IR- vs RAS-induced senescent fibroblasts were largely distinct, sharing only 9 significantly altered proteins (**Figure 5D**). Exosomes/EVs were reported to contain protein signatures of their originating cells (Belov et al., 2016; Takasugi, 2018), presenting a unique opportunity to develop senescence biomarkers with a degree of specificity. As suggested by our proteomic analysis, exosome/EV cargo proteins might distinguish senescent cells of different origins or originating from different stressors. The membrane protein topology of exosomes is also representative of their originating cells (Belov et al., 2016; Takasugi, 2018). About 30% of all the exosome/EV proteins that increased upon senescence are plasma membrane proteins (**Figure 5E**). Therefore, the identification of plasma membrane proteins associated with exosomes/EVs might also serve to identify cell-surface proteins expressed on senescent cells. There are currently no reliable senescence-specific cell-surface markers, and so the identification of these markers would be very valuable for isolating or therapeutically targeting senescent cells.

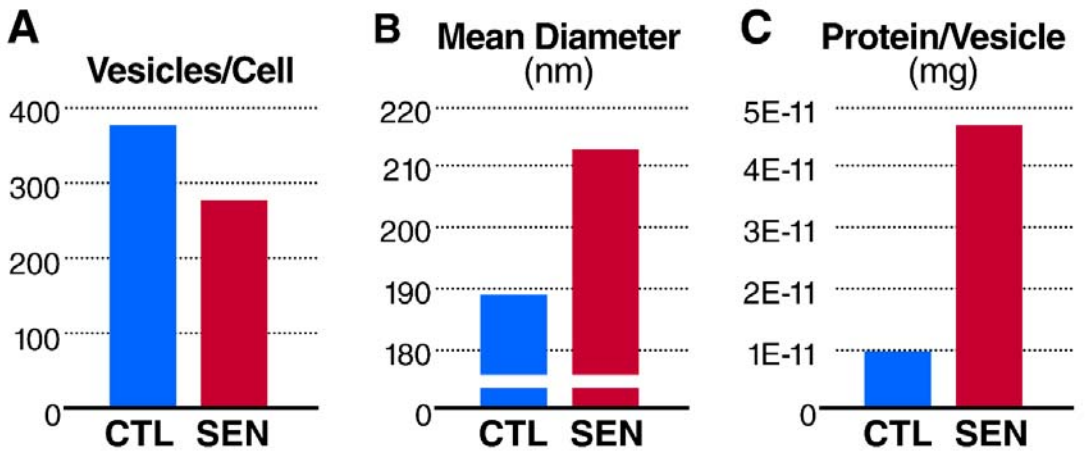

D

Genes	IR Fold Change SEN/CTL	RAS Fold Change SEN/CTL
ANXA1	1.43	6.19
ANXA2	1.82	2.91
ENO3	1.52	1.13
AHNAK	1.21	4.92
SLC1A5	3.71	6.11
ITGA1	–1.52	–1.77
COL6A2	–5.56	–2.32
COL6A1	–5.71	–3.26
COL6A3	–5.65	–6.87

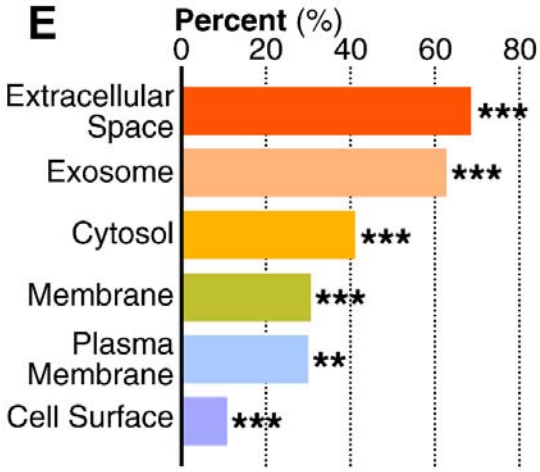

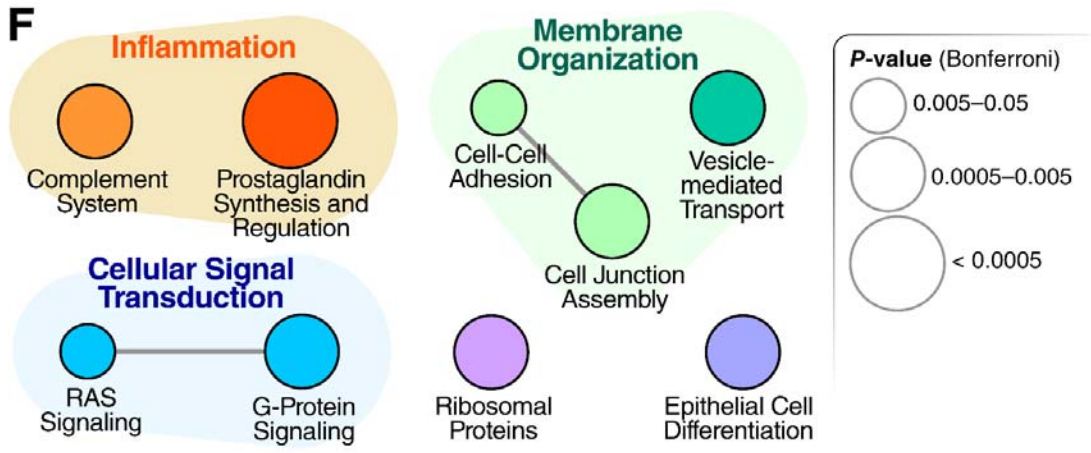

Figure 5. Cellular senescence alters exosome/EV biology and composition. Based on size distribution analyses, senescent cells release A) fewer exosomes/EVs per cell, but with B) larger volumes and C) higher protein contents. D) Table showing overlapping protein changes in exosomes/EVs secreted by senescent cells induced by IR vs RAS. E) Enrichment analysis of gene-ontology/cellular compartments overrepresented among the protein contents of exosomes/EVs released by senescent cells. F) Network analysis of pathways and functions unique to the eSASP.

The SASP Contains Potential Aging and Disease Biomarkers

As a driver of many aging and disease phenotypes, we hypothesized that the SASP would include known biomarkers of aging and age-related diseases. A recent proteomic biomarker study in a human cohort reported 217 proteins that are significantly associated with age in human plasma (Tanaka et al., 2018). Of these markers, the authors noted that 20 proteins (9.2%) are present in the originally-defined SASP (Coppé et al., 2008). Strikingly, multiple newly identified SASP factors from our study were also identified by Tanaka et al. as age-associated. Considering our newly identified "core SASP" -- SASP components resulting from all senescence inducers -- the number of age-associated plasma proteins that are also SASP proteins, doubles to 40 proteins (18.4%, **Table S4**). If all novel SASP proteins we identified are considered, over a third (36.9%) of age-related changes in plasma proteins are also highly secreted by senescent cells, (**Table S4**). Thus, plasma biomarkers of aging are highly enriched with SASP factors. Notably, the protein having the strongest association with aging reported by Tanaka et al., GDF15 (r=0.82), was among the most highly secreted proteins in the sSASP induced by IR, RAS and ATV in fibroblasts, and

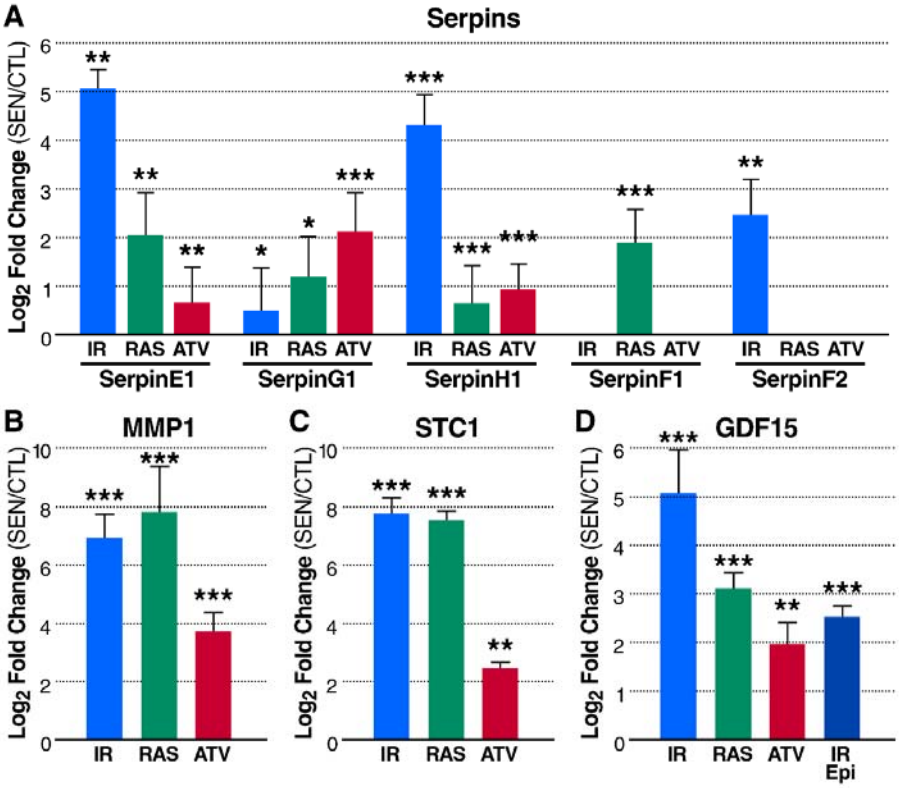

Figure 6. The SASP contains aging and disease biomarkers. A) Serpins are secreted at high levels by senescent fibroblasts induced by IR, RAS and ATV. B) MMP1 and C) STC1 are among the most highly secreted proteins by senescent fibroblasts. D) The plasma aging biomarker GDF15 is increased in the sSASPs of fibroblasts induced to senesce by IR, RAS and ATV and epithelial cells induced to senesce by IR. IR = X-irradiation, RAS = RAS oncogene overexpression, ATV = atazanavir treatment, Epi = renal epithelial cells. *q < 0.05, **q < 0.01, ***q < 0.001.

epithelial cells induced by IR (**Figure 6A**). In addition to aging, various large cohort studies identified GDF15 as a biomarker of cardiovascular disease, cardiovascular and cancer mortality and morbidity, renal disease, and all-cause mortality independent of cardiovascular mortality (Bidadkosh et al., 2017; Daniels et al., 2011; Ho et al., 2012, 2013; Rohatgi et al., 2012; Wallentin et al., 2013; Wollert et al., 2017).

Complement and coagulation cascade proteins, particularly those with protease inhibitor activity such as SERPINs, were also noted as prominent plasma biomarkers of aging (Tanaka et al., 2018). Notably, these proteins and their pathway networks were robustly altered in the SASPs of cells induced to senesce by multiple stressors (**Figure 3C, Figure 6B**). Additionally, two of the top "core sSASP" proteins identified by an unbiased k-means clustering algorithm – STC1 and MMP1 (**Figure 6C-D**) – were reported as significant aging biomarkers (Tanaka et al., 2018). In addition to aging, MMP1 has been identified as a biomarker for several cancers, pulmonary fibrosis, and potentially Alzheimer's disease (Bhat et al., 2012; Chen et al., 2016; Rosas et al., 2008; Roy et al., 2009), whereas STC1 has been identified as a diagnostic and prognostic biomarker for cancers, pulmonary fibrosis, renal ischemia/reperfusion injury, and Alzheimer's disease (Chang et al., 2015; Du et al., 2016; Ohkouchi et al., 2015; Pan et al., 2015; Shahim et al., 2017; Su et al., 2015). The enrichment of aging and disease biomarkers in the secretomes of senescent cells supports their links to a wide spectrum of age-related diseases and highlights the need for comprehensive secretome profiles of senescent cells in multiple biological contexts.

SASP Atlas and Proteomics Assays for Biomarker Discovery and Identification of Secretory Phenotypes

Here we present SASP Atlas (www.SASPAtlas.com), the first proteome-based database of SASPs. This comprehensive and unbiased database contains exosome/EV and soluble secretomes, in addition to SASPs originating from multiple senescence-inducing stresses and cell types. The SASP Atlas will be continuously updated with SASP profiles from new cell types and inducers of senescence, including paracrine (or "bystander") senescence (Acosta et al., 2013; Nelson et al., 2012), as well as temporal dynamics of the SASP – all generated by our laboratories. In addition to a

database, we created proteomic 'secretome panels' on Panorama Web (Sharma et al., 2018), a freely-available repository server for targeted mass spectrometry assays as a resource for others to detect and quantify the SASP in mass spectrometry studies. These resources can be used both as a reference and a guide to pinpoint and quantify SASP factors that may be associated with diseases of interest, and to develop aging and disease-related biomarkers (**Figure 7**).

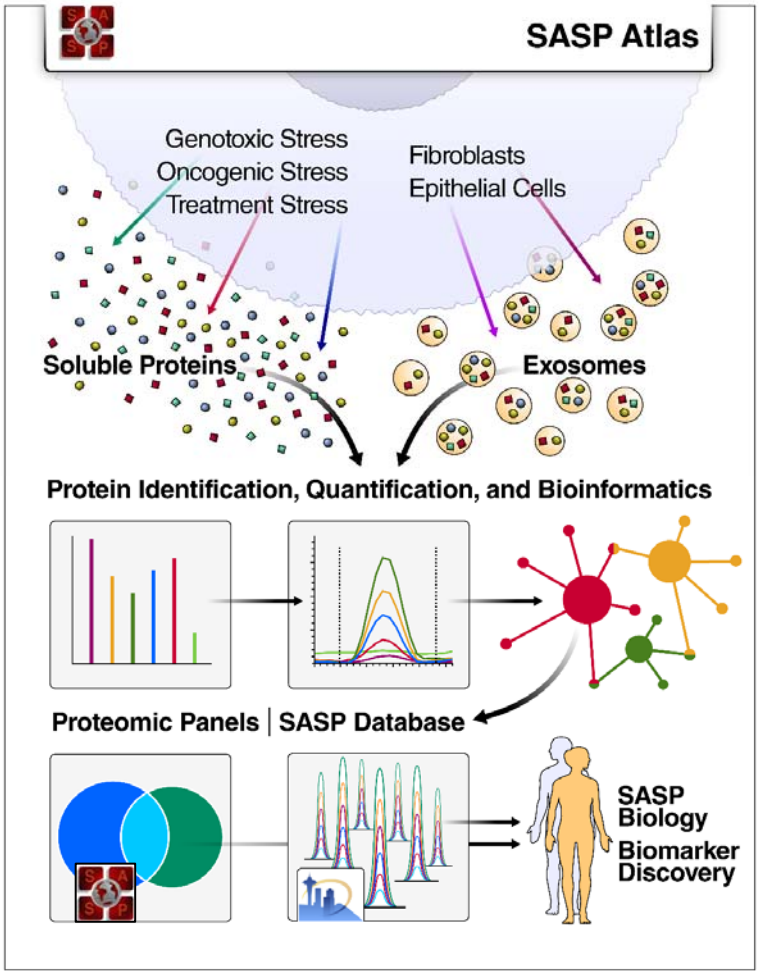

Figure 7. SASP Atlas: A Comprehensive Resource for Senescence-Associated Secretory Phenotypes. SASP Atlas (www.SASPAtlas.com) is a curated and freely-available database of the secretomes of senescent cells, including both the soluble SASP and exosome SASP. This resource may be referenced to identify SASP SASP components or potential biomarker candidates for senescence burden, aging, and related diseases. Proteomic SASP panels are also available online for targeted extraction and quantification of SASP components from proteomic data.

SASP profiles are needed to develop senescence biomarkers in human plasma or other biofluids and are critical for identifying individuals to treat with, and measuring the efficacy of, senescence-targeted therapies such as senolytics. Translating senescence- and SASP-targeting interventions to humans will require a comprehensive profile of SASPs, both to identify the deleterious components of the SASP and to develop human biomarkers to assess senescent cell burden. The SASP, as originally identified, comprised ~50 cytokines, chemokines, growth factors, and proteases that were detected by biased methods (e.g., antibody arrays) and/or transcriptional analyses (Acosta et al., 2008; Coppé et al., 2008,

2010a; Kuilman et al., 2008). Transcriptomic profiling has also been performed on senescent cells (Hernandez-Segura et al., 2017). While these unbiased comprehensive analyses are valuable in describing the overall phenotype of senescent cells, they cannot accurately portray the secreted protein profile with quantitative accuracy. For example, a recent meta-analysis of senescent cell transcriptomes identified 21 core SASP mRNAs expressed by senescent fibroblasts, whereas we found 172 core SASP proteins, with only a small fraction of all protein-level changes being identified by transcriptomics (**Figure S4**). Of course, the number and nature of these core proteins will change as we and others interrogate additional cell types and senescence inducers. Additionally, the secretion of SASP factors such as HMGB1 and other DAMPs is not generally transcriptionally driven.

Our quantitative and unbiased *proteomic* analysis of senescent fibroblasts and epithelial cells clearly reveals a much larger and diverse SASP than initially reported. These SASP profiles contribute a number of new potential senescence, aging, and disease biomarkers. In addition to general senescence biomarkers, many protein markers will likely be specific to cell-type and originating stimulus. Thus, biomarkers present in human patients *in vivo* will likely vary depending on the affected tissue, originating cell types, and senescence stimuli. Therefore, comprehensive quantitative profiles of the SASP under a variety of physiological conditions will provide biomarker candidates with a higher degree of selectivity to specific *in vivo* pathologies in humans.

METHODS

KEY RESOURCES TABLE

REAGENT or RESOURCE	SOURCE	IDENTIFIER
Chemicals, Peptides, and Recombinant Proteins		
Atazanavir	MedChemExpress	HY-17367
Pen-Strep	Gibco	15070063
DMEM	Gibco	12430-054
Trypsin-EDTA	Corning	25-051-CI
Fetal Bovine Serum	Gibco	2614079
PBS	Gibco	10010-23
DMEM (phenol-red-free)	Gibco	21063-029
Acetonitrile (HPLC grade)	Burdick & Jackson	AH015
Water (HPLC grade)	Burdick & Jackson	AH365
Iodoacetamide	Sigma	I1149
Dithiothreitol	Sigma	D9779
Formic Acid	Sigma	94318
Triethylammonium bicarbonate	Sigma	T7408
Urea	Thermo Scientific	29700
Trypsin (sequencing grade)	Promega	V5113
HLB Oasis SPE cartridges	Waters	186003908
Amicon Ultra-15 Centrifugal Filter Units, 3kDa	MilliporeSigma	UFC900324
Hyper Reaction Monitoring Peptide Standards	Biognosys	Kit-3003
Sytox Green	Invitrogen	S7020
DNase I Amp	Invitrogen	18068015
Critical Commercial Assays		
Senescence-Associated-Beta-Galactosidase Staining Kit	BioVision	K320-250
BCA Protein Assay Kit	Pierce	23225
Lenti-X™ Tet-On® Advanced Inducible Expression System	Clontech	632162
PureLink Micro-to-Midi total RNA Purification System	Invitrogen	12183018A
High-Capacity cDNA Reverse Transcription Kit	Applied Biosystems	4368813

Deposited Data		
SASP Database	This paper	www.SASPAtlas.com
Proteomic SASP Panels	This paper, Panorama	https://panoramaweb.org/project/Schilling/SASP_Atlas_Buck/begin.view?
Proteomics data	This paper, MassIVE	MSV000083468
Pan-Human Spectral Library	Rosenberger et al., 2014	
Human Proteome (https://www.uniprot.org/uniprot/?query=human&fil=reviewed%3Ayes+AND+organism%3A%22Homo+sapiens+%28Human%29+%5B9606%5D%22+AND+proteome%3Aup000005640&sort=score)	UniProt	UP00005640
Plasma Aging Biomarkers	Tanaka et al., 2018	
Gene Ontology	The Gene Ontology Resource	
Human Kegg pathways	KEGG PATHWAY Database	
Human WikiPathways	WikiPathways	
Human Reactome Pathways	Reactome Pathway Database	
Experimental Models: Cell Lines		
IMR90 primary human lung fibroblasts	ATCC	CCL-186
human primary renal cortical epithelial cells (HRCE)	ATCC	PCS-400-011
Software and Algorithms		
Spectronaut X (version 12)	Biognosys, Rosenberger et al, 2014	https://www.biognosys.com/shop/spectronaut-x
Cytoscape (version 3.7.1)	Shannon et al., 2003	https://cytoscape.org/
ClueGO (version 2.5.3)	Bindea et al., 2009	http://apps.cytoscape.org/apps/cluego
R (version 3.5.2)	R Development Core Team, 2011	https://www.r-project.org, RRID:SCR_001905
Rstudio (version 1.0.136)	Rstudio: Integrated Development for R. RStudio, Boston, MA	https://www.rstudio.com/, RRID:SCR_000432
VennDiagram (R)	Chen, 2018	https://cran.r-project.org/web/packages

		/VennDiagram/index.html
gplots (R)	Warnes et al., 2019	https://cran.r-project.org/web/packages/gplots/index.html
RColorBrewer (R)	Neuwirth, 2014	https://cran.r-project.org/web/packages/RColorBrewer/index.html
Scikit-learn (Python)	Pedregosa et al., 2011	https://scikit-learn.org/stable/
Other		
SASP Atlas	This paper	www.SASPAtlas.com

CONTACT FOR REAGENT AND RESOURCE SHARING

Further information and requests for resources and reagents should be directed to and will be fulfilled by the Lead Contact, Birgit Schilling (bschilling@buckinstitute.org).

EXPERIMENTAL MODEL AND SUBJECT DETAILS

Human Cell Culture and Primary Cell Lines

IMR90 primary human lung fibroblasts (Female, ATCC #CCL186) were cultured in Dulbecco's Modified Eagle's Medium (DMEM, Gibco #12430-054) supplemented with Penicillin Streptomycin (5000 U/mL penicillin and 5000 µg/mL streptomycin, Gibco #15070063) and 10% Fetal Bovine Serum (Gibco #2614079) and maintained at 37° C, 10% CO_2, and 3% O_2. Primary human renal epithelial cells (ATCC PCS400011) were cultured in Renal Epithelial Cell Basal Medium (Female, ATCC #PCS-400-030) and maintained at 37° C, 10% CO_2, and 3% O_2.

Induction of Senescence

X-ray irradiation: Induction of senescence by ionizing radiation (IR) was performed with 10 Gy X-ray. Quiescent control cells were mock irradiated. Senescent cells were cultured for 10 days to allow development of the senescent phenotype, and quiescent cells were cultured in 0.2% serum for 3 days. Subsequently, cells were washed with PBS (Gibco #10010-023) and placed in serum-free and phenol-red-free DMEM (Gibco

#21063-029) and conditioned media was collected after 24 hours to obtain the secreted protein fractions.

RAS overexpression: RAS^{v12} was cloned in pLVX vector (Lenti-X™ Tet-On from Clontech #632162) to make lentivirus. The Lenti-X Tet-On Advanced Inducible Expression System is a lentiviral-based gene transfer technology to deliver inducible gene expression system into dividing and nondividing target cells, primary cells, and stem cells. Lentivirus were then generated and collected from 293FT cells and used for transduction to IMR-90 cells (PD-30). Transduced cells were selected with puromycin (1 µg/ml) for 24 hours. Stable IMR-90 cells carrying inducible RAS^{v12} were generated and used for further experiments. For induction of RAS^{v12}, cells were treated with 1 µg/ml Doxycycline dissolved in DMSO (Sigma # D9891) for 4 days (early time point) or 7 days, which is optimal for senescence induction. Doxycycline was replaced after every 48 hours in the induction medium Subsequently, cells were washed with PBS (Gibco #10010-023) and placed in serum-free and phenol-red-free DMEM (Gibco #21063-029) and conditioned media was collected after 24 hours to obtain the secreted protein fractions.

Atazanivir treatment: Induction of senescence was performed with a clinically relevant dose (20 µM) of Atazanavir. Cells were grown in appropriate media containing Atazanavir or vehicle (DMSO) for 9 days (early timepoint) or 14 days, which is optimal for senescence induction. Subsequently, cells were washed with PBS (Gibco #10010-023) and placed in serum-free and phenol-red-free DMEM (Gibco #21063-029) and conditioned media was collected after 24 hours to obtain the secreted protein fractions.

Isolation of Secreted Soluble Proteins and Exosomes/EVs:

Proteins secreted into serum-free medium over a 24-hr period were collected for each experimental condition. An ultracentrifugation-based protocol was used to separate the exosome and small extracellular vesicle fraction from the soluble protein fraction (Théry et al., 2006). Briefly, conditioned medium containing secreted proteins was centrifuged at 10,000 x g at 4° C for 30 minutes to remove cellular debris. The supernatant was

then centrifuged at 20,000 x g at 4° C for 70 minutes to remove microvesicles. The supernatant was then ultracentrifuged at 100,000 x g at 4° C for 70 minutes to pellet exosomes. The exosome-depleted supernatant was saved for proteomic sample preparation. The exosome pellet was then washed and ultracentrifuged at 100,000 x g at 4° C for 70 minutes two times with PBS before resuspending the exosome pellet in PBS and saved for proteomic sample preparation.

Proteomic Sample Preparation

Chemicals: Acetonitrile (#AH015) and water (#AH365) were obtained from Burdick & Jackson (Muskegon, MI). Reagents for protein chemistry including iodoacetamide (IAA, #I1149), dithiothreitol (DTT, #D9779), formic acid (FA, #94318-50ML-F), and Triethylammonium bicarbonate buffer 1.0 M, pH 8.5±0.1 (#T7408) were purchased from Sigma Aldrich (St. Louis, MO). Urea (#29700) was purchased Thermo Scientific (Waltham, MA). Sequencing grade trypsin (#V5113) was purchased from Promega (Madison, WI). HLB Oasis SPE cartridges (#186003908) were purchased from Waters (Milford, MA).

Protein concentration and quantification: Samples were concentrated using Amicon Ultra-15 Centrifugal Filter Units with 3 kDa molecular weight cutoff (MilliporeSigma #UFC900324) per manufacturer instructions and transferred into a solution of 8M urea/50 mM Triethylammonium bicarbonate buffer at pH 8. Protein quantitation was then performed using a BCA Protein Assay Kit (Pierce #23225, Waltham, MA).

Digestion: An aliquot of 25-100 µg from each sample was then brought to equal volume with 50 mM Triethylammonium bicarbonate buffer at pH 8. The protein mixtures were reduced with 20 mM DTT (37°C for 1 hour), and subsequently alkylated with 40 mM iodoacetamide (30 minutes at RT in the dark). Samples were diluted 10-fold with 50 mM Triethylammonium bicarbonate buffer at pH 8 and incubated overnight at 37°C with sequencing grade trypsin (Promega) added at a 1:50 enzyme:substrate ratio (wt/wt).

Desalting: The peptide supernatants were then collected and desalted with Oasis HLB 30 mg Sorbent Cartridges (Waters #186003908, Milford, MA), concentrated, and re-suspended in a solution containing mass spectrometric 'Hyper Reaction Monitoring' peptide standards (HRM, Biognosys #Kit-3003, Switzerland) and 0.2% formic acid in water.

Mass Spectrometry Analysis

Samples were analyzed by reverse-phase HPLC-ESI-MS/MS using the Eksigent Ultra Plus nano-LC 2D HPLC system (Dublin, CA) combined with a cHiPLC System, which was directly connected to a quadrupole time-of-flight SCIEX TripleTOF 6600 or a TripleTOF 5600 mass spectrometer (SCIEX, Redwood City, CA). Typically, mass resolution in precursor scans was ~ 45,000 (TripleTOF 6600), while fragment ion resolution was ~15,000 in 'high sensitivity' product ion scan mode. After injection, peptide mixtures were transferred onto a C18 pre-column chip (200 µm x 6 mm ChromXP C18-CL chip, 3 µm, 300 Å, SCIEX) and washed at 2 µl/min for 10 min with the loading solvent (H_2O/0.1% formic acid) for desalting. Subsequently, peptides were transferred to the 75 µm x 15 cm ChromXP C18-CL chip, 3 µm, 300 Å, (SCIEX), and eluted at a flow rate of 300 nL/min with a 3 h gradient using aqueous and acetonitrile solvent buffers.

For label-free relative quantification all study samples were analyzed by data-independent acquisitions (DIA), or specifically variable window SWATH acquisitions. In these SWATH acquisitions, instead of the Q1 quadrupole transmitting a narrow mass range through to the collision cell, windows of variable width (5 to 90 m/z) are passed in incremental steps over the full mass range (m/z 400-1250). The cycle time of 3.2 sec includes a 250 msec precursor ion scan followed by 45 msec accumulation time for each of the 64 SWATH segments. The variable windows were determined according to the complexity of the typical MS1 ion current observed within a certain m/z range using a SCIEX 'variable window calculator' algorithm (i.e. more narrow windows were chosen in 'busy' m/z ranges, wide windows in m/z ranges with few eluting precursor ions) (Schilling et al., 2017). SWATH MS2 produces complex MS/MS spectra which are a

composite of all the analytes within each selected Q1 m/z window. This method requires high scan speeds and high-resolution capabilities, as well as a 'reference spectral library' that can be either generated in-house or taken from existing comprehensive and large-scale studies. All collected mass spectrometry data was processed in Spectronaut using pan-human library that provides SWATH assays for ~10,000 human proteins (Rosenberger et al., 2014).

Cell Viability Assays

Cell viability was assessed with SYTOX Green Nucleic Acid Stain (Invitrogen #S7020). Senescent and control cells over a 24-hour period in serum-free medium containing SYTOX Green with continuous imaging. Cell death was quantified by counting total SYTOX Green positive nuclei appearing in a 24-hour time-lapse video.

Senescence-Associated β-Galactosidase Staining

Senescence-associated beta-galactosidase (SA-β-gal) activity was determined using the BioVision Senescence Detection Kit (Cat# K320-250) protocol. For each experiment, approximately 100–150 cells were counted.

RNA Extraction and quantitative Real-Time PCR

Total RNA was prepared using the PureLink Micro-to-Midi total RNA Purification System (Invitrogen # 12183018A), according to the manufacturer's protocol. Samples were treated with DNase I Amp Grade (Invitrogen #18068015) before retrotranscription to eliminate genomic DNA contamination. RNA was reverse transcribed into cDNA using a High-Capacity cDNA Reverse Transcription Kit (Applied Biosystems #4368813), according to the manufacturer's protocol. Quantitative RT-PCR (qRT-PCR) reactions were performed as described using the Universal Probe Library system (Roche). The Actin and Tubulin predeveloped TaqMan assays (Applied Biosystems) were used to control for cDNA quantity. Quantitative RT-PCR assays were performed on the LightCycler 480 Sytem (Roche, Basel, Switzerland). The primers and probes were as follows:

Human actin F 5'- CCAACCGCGAGAAGATGA; R 5'- TCCATCACGATGCCAGTG, UPL probe #64

Human tubulin F 5'- CTTCGTCTCCGCCATCAG; R 5'- TTGCCAATCTGGACACCA, UPL Probe #58

Human IL-6 F 5'- GCCCAGCTATGAACTCCTTCT; R 5'- GAAGGCAGCAGGCAACAC, UPL Probe #45

Human $p16^{INK4a}$ F 5'-GAGCAGCATGGAGCCTTC; R 5'-CGTAACTATTCGGTGCGTTG, UPL Probe #34

Exosome Size Distribution Analysis

Particle diameter and concentration were assessed using an IZON qNano Nanoparticle Characterization instrument (Zen-bio, Inc., Research Triangle Park, NC).

QUANTIFICATION AND STATISTICAL ANALYSIS

Processing, Quantification, and Statistical Analysis of MS Data

SWATH acquisitions were quantitatively processed using the proprietary Spectronaut v12 (12.020491.3.1543) software (Bruderer et al., 2015) from Biognosys. Quantitative SWATH MS2 data analysis was based on extracted ion chromatograms (XICs) of 6-10 of the most abundant fragment ions in the identified spectra. Relative quantification was performed comparing different conditions (senescent versus control) assessing fold changes for proteins from the investigated cells and conditions. The number of replicates from proteomic each experiment are as follows: X-ray irradiated fibroblasts, 4 senescent and 4 control replicates; X-ray irradiated renal epithelial cells, 5 senescent and 5 control replicates; 4 day RAS-induction in fibroblasts, 10 senescent and 10 control replicates; 7 day RAS-induced fibroblasts, 6 senescent and 6 control replicates; atazanavir-treated fibroblasts, 3 senescent (9 days treatment), 3 senescent (14 days treatment), and 4 control replicates; X-ray irradiated fibroblast exosomes, 5 senescent and 5 control replicates; 7 day RAS-induced fibroblast exosomes, 6 senescent and 6 control replicates. Significance was assessed using FDR corrected q-values<0.05. See Data Accession (below) for quantitative results from mass spectrometric SWATH analysis.

Pathway and Network Analysis

Gene ontology, pathway, and network analysis was performed using the GlueGO package version 2.5.3 in Cytoscape version 3.7.1 (Bindea et al., 2009; Shannon et al., 2003). Curated pathways for enrichment analysis were referenced from the following databases: GO Biological Function, GO Cellular Compartment, Kegg pathways, WikiPathways, and Reactome Pathways. For gene ontology data, testing was restricted to pathways with experimental evidence (EXP, IDA, IPI, IMP, IGI, IEP). The statistical cutoff for enriched pathways was Bonferroni-adjusted p-values < 0.01 by right-sided hypergeometric testing. Pathway-connecting edges were drawn for kappa scores > 40%. Kappa scores are a measure of inter-pathway agreement among observed proteins that indicate whether pathway agreement is greater than expected by chance based on shared proteins. Pathways with the same color indicate >= 50% similarity in terms.

K-Means Clustering

Unsupervised clustering was performed in Python with Scikit-learn, a module integrating a wide range of machine learning algorithms (Pedregosa et al., 2011). Datasets were pre-processed with the StandardScaler function and clustered with the KMeans algorithm.

Data Visualization

Heatmaps were visualized in R using the heatmap.2 function in the ‘gplots’ package (Warnes et al., 2019). Venn diagrams were visualized with the “VennDiagram” package in R (Chen, 2018). Color palettes in R were generated with the “RColorBrewer” package (Neuwirth, 2014). Pathway and network visualizations were generated and modified using the GlueGO package in Cytoscape (Bindea et al., 2009; Shannon et al., 2003).

DATA AND SOFTWARE AVAILABILITY

Data availability: All raw files are uploaded to the Center for Computational Mass Spectrometry, MassIVE, and can be downloaded using the following ftp link

ftp://massive.ucsd.edu/MSV000083468 (MassIVE ID number: MSV00008346). Data uploads include the protein identification and quantification details, spectral library, and FASTA file used for mass spectrometric analysis. Proteomic assays of SASP profiles are available on Panorama (https://panoramaweb.org/project/Schilling/SASP_Atlas_Buck/begin.view?), a repository for targeted mass spectrometry assays generated in Skyline software (Sharma et al., 2014, 2018). All quantitative data is available for viewing and downloading on SASP Atlas (www.saspatlas.com).

MassIVE: MSV000083468 **(**ftp://massive.ucsd.edu/MSV000083468)
SASP Atlas: www.SASPAtlas.com
SASP Panels:
https://panoramaweb.org/project/Schilling/SASP_Atlas_Buck/begin.view?

SUPPLEMENTAL INFORMATION

Supplemental Information includes 4 figures, 4 tables:

- **Supplemental Table 1**: Mass spectrometry quantification outputs for each dataset, as separate worksheets in a single excel workbook.
- **Supplemental Table 2**: Proteins with increased secretion in all senescence-inducing stresses.
- **Supplemental Table 3**: Proteins with increased secretion in all cell types and senescence-inducing stresses.
- **Supplemental Table 4**: Age-associated plasma proteins in the SASP
- **Supplemental Figure 1**: Senescence-associated β-galactosidase staining and expression of senescence markers.
- **Supplemental Figure 2**: Cell Viability Assays.
- **Supplemental Figure 3**: Exosome/EV proteomic markers and size distribution analysis.
- **Supplemental Figure 4**: Comparison of our proteomic data with transcriptional changes in senescent cells.

AKNOWLEDGMENTS

This work was supported by the National Institute on Aging (U01 AG060906-01, PI: Schilling; and P01AG017242 and R01AG051729, PI: Campisi) and National Institute of Health Shared Instrumentation Grant (1S10 OD016281, Buck Institute). N.B. and O.J. were supported by postdoctoral fellowships from the Glenn Foundation for Medical Research. A.K. was supported by the SENS Foundation. We thank John C.W. Carroll for help creating figures.

AUTHOR CONTRIBUTIONS

Conceptualization, N.B., B.S., J.C. L.F.; Cell Culture, N.B., A.K., O.J., C.K., T.P.; RNA expression and Activity Assays, N.B., A.K., O.J., C.K. T.P.; Proteomic Sample Preparation, N.B., T.P., A.H., S.S.; Data Analysis, N.B., B.S., A.H., S.S.; Pathway and Network Analysis, N.B., C.R.; Visualization, N.B., C.R.; Web Database, C.R., N.B, B.S; Writing and Editing, N.B., B.S., J.C., L.F.; Funding Acquisition, B.S., J.C.

DECLARATION OF INTERESTS

The authors declare no competing interests.

REFERENCES

Abdul-Aziz, A.M., Sun, Y., Hellmich, C., Marlein, C.R., Mistry, J., Forde, E., Piddock, R.E., Shafat, M.S., Morfakis, A., Mehta, T., et al. (2018). Acute myeloid leukemia induces pro-tumoral p16INK4a driven senescence in the bone marrow microenvironment. Blood *133*, 446–456.

Acosta, J.C., O'Loghlen, A., Banito, A., Guijarro, M.V., Augert, A., Raguz, S., Fumagalli, M., Da Costa, M., Brown, C., Popov, N., et al. (2008). Chemokine signaling via the CXCR2 receptor reinforces senescence. Cell *133*, 1006–1018.

Acosta, J.C., Banito, A., Wuestefeld, T., Georgilis, A., Janich, P., Morton, J.P., Athineos, D., Kang, T.W., Lasitschka, F., Andrulis, M., et al. (2013). A complex secretory program orchestrated by the inflammasome controls paracrine senescence. Nat Cell Biol *15*, 978–990.

Baar, M.P., Brandt, R.M.C., Putavet, D.A., Klein, J.D.D., Derks, K.W.J., Bourgeois, B.R.M., Stryeck, S., Rijksen, Y., van Willigenburg, H., Feijtel, D.A., et al. (2017). Targeted Apoptosis of Senescent Cells Restores Tissue Homeostasis in Response to Chemotoxicity and Aging. Cell *169*, 132-147.e16.

Baker, D.J., Wijshake, T., Tchkonia, T., LeBrasseur, N.K., Childs, B.G., van de Sluis, B., Kirkland, J.L., and van Deursen, J.M. (2011). Clearance of $p16^{Ink4a}$-positive senescent cells delays ageing-associated disorders. Nature *479*, 232–236.

Baker, D.J., Childs, B.G., Durik, M., Wijers, M.E., Sieben, C.J., Zhong, J., Saltness, R.A., Jeganathan, K.B., Verzosa, G.C., Pezeshki, A., et al. (2016). Naturally occurring p16(Ink4a)-positive cells shorten healthy lifespan. Nature *530*, 184–189.

Belov, L., Matic, K.J., Hallal, S., Best, O.G., Mulligan, S.P., and Christopherson, R.I. (2016). Extensive surface protein profiles of extracellular vesicles from cancer cells may provide diagnostic signatures from blood samples. J Extracell Vesicles *5*.

Bhat, R., Crowe, E.P., Bitto, A., Moh, M., Katsetos, C.D., Garcia, F.U., Johnson, F.B., Trojanowski, J.Q., Sell, C., and Torres, C. (2012). Astrocyte senescence as a component of Alzheimer's disease. PLoS ONE *7*, e45069.

Bidadkosh, A., Lambooy, S.P.H., Heerspink, H.J., Pena, M.J., Henning, R.H., Buikema, H., and Deelman, L.E. (2017). Predictive Properties of Biomarkers GDF-15, NTproBNP, and hs-TnT for Morbidity and Mortality in Patients With Type 2 Diabetes With Nephropathy. Diabetes Care *40*, 784–792.

Bindea, G., Mlecnik, B., Hackl, H., Charoentong, P., Tosolini, M., Kirilovsky, A., Fridman, W.-H., Pagès, F., Trajanoski, Z., and Galon, J. (2009). ClueGO: a Cytoscape plug-in to decipher functionally grouped gene ontology and pathway annotation networks. Bioinformatics *25*, 1091–1093.

Bonifati, V., Rizzu, P., van Baren, M.J., Schaap, O., Breedveld, G.J., Krieger, E., Dekker, M.C.J., Squitieri, F., Ibanez, P., Joosse, M., et al. (2003). Mutations in the DJ-1 gene associated with autosomal recessive early-onset parkinsonism. Science *299*, 256–259.

Bruderer, R., Bernhardt, O.M., Gandhi, T., Miladinović, S.M., Cheng, L.Y., Messner, S., Ehrenberger, T., Zanotelli, V., Butscheid, Y., Escher, C., et al. (2015). Extending the limits of quantitative proteome profiling with data-independent acquisition and application to acetaminophen-treated three-dimensional liver microtissues. Mol Cell Proteomics *14*, 1400–1410.

Chang, A.C.-M., Doherty, J., Huschtscha, L.I., Redvers, R., Restall, C., Reddel, R.R., and Anderson, R.L. (2015). STC1 expression is associated with tumor growth and metastasis in breast cancer. Clin. Exp. Metastasis *32*, 15–27.

Chang, J., Wang, Y., Shao, L., Laberge, R.M., Demaria, M., Campisi, J., Janakiraman, K., Sharpless, N.E., Ding, S., Feng, W., et al. (2016). Clearance of senescent cells by ABT263 rejuvenates aged hematopoietic stem cells in mice. Nat Med *22*, 78–83.

Chen, H. (2018). VennDiagram: Generate High-Resolution Venn and Euler Plots.

Chen, Y.-K., Tung, C.-W., Lee, J.-Y., Hung, Y.-C., Lee, C.-H., Chou, S.-H., Lin, H.-S., Wu, M.-T., and Wu, I.-C. (2016). Plasma matrix metalloproteinase 1 improves the detection and survival prediction of esophageal squamous cell carcinoma. Scientific Reports *6*, 30057.

Childs, B.G., Baker, D.J., Wijshake, T., Conover, C.A., Campisi, J., and van Deursen, J.M. (2016). Senescent intimal foam cells are deleterious at all stages of atherosclerosis. Science *354*, 472–477.

Coppé, J.-P., Patil, C.K., Rodier, F., Sun, Y., Muñoz, D.P., Goldstein, J., Nelson, P.S., Desprez, P.-Y., and Campisi, J. (2008). Senescence-Associated Secretory Phenotypes Reveal Cell-Nonautonomous Functions of Oncogenic RAS and the p53 Tumor Suppressor. PLOS Biology *6*, e301.

Coppé, J.-P., Patil, C.K., Rodier, F., Krtolica, A., Beauséjour, C.M., Parrinello, S., Hodgson, J.G., Chin, K., Desprez, P.-Y., and Campisi, J. (2010a). A Human-Like Senescence-Associated Secretory Phenotype Is Conserved in Mouse Cells Dependent on Physiological Oxygen. PLoS One *5*, e9188.

Coppé, J.-P., Desprez, P.-Y., Krtolica, A., and Campisi, J. (2010b). The Senescence-Associated Secretory Phenotype: The Dark Side of Tumor Suppression. Annu Rev Pathol *5*, 99–118.

Daniels, L.B., Clopton, P., Laughlin, G.A., Maisel, A.S., and Barrett-Connor, E. (2011). Growth-differentiation factor-15 is a robust, independent predictor of 11-year mortality risk in community-dwelling older adults: the Rancho Bernardo Study. Circulation *123*, 2101–2110.

Davalos, A.R., Kawahara, M., Malhotra, G.K., Schaum, N., Huang, J., Ved, U., Beausejour, C.M., Coppe, J.-P., Rodier, F., and Campisi, J. (2013). p53-dependent release of Alarmin HMGB1 is a central mediator of senescent phenotypes. J. Cell Biol. *201*, 613–629.

Demaria, M., Ohtani, N., Youssef, S.A., Rodier, F., Toussaint, W., Mitchell, J.R., Laberge, R.-M., Vijg, J., Van Steeg, H., Dollé, M.E.T., et al. (2014). An Essential Role for Senescent Cells in Optimal Wound Healing through Secretion of PDGF-AA. Dev Cell *31*, 722–733.

Demaria, M., O'Leary, M.N., Chang, J., Shao, L., Liu, S., Alimirah, F., Koenig, K., Le, C., Mitin, N., Deal, A.M., et al. (2017). Cellular Senescence Promotes Adverse Effects of Chemotherapy and Cancer Relapse. Cancer Discov *7*, 165–176.

Du, Y.-Z., Gu, X.-H., Cheng, S.-F., Li, L., Liu, H., Hu, L.-P., and Gao, F. (2016). The oncogenetic role of stanniocalcin 1 in lung adenocarcinoma: a promising serum candidate biomarker for tracking lung adenocarcinoma progression. Tumour Biol. *37*, 5633–5644.

Egertson, J.D., MacLean, B., Johnson, R., Xuan, Y., and MacCoss, M.J. (2015). Multiplexed peptide analysis using data-independent acquisition and Skyline. Nature Protocols *10*, 887.

Eitan, E., Green, J., Bodogai, M., Mode, N.A., Bæk, R., Jørgensen, M.M., Freeman, D.W., Witwer, K.W., Zonderman, A.B., Biragyn, A., et al. (2017). Age-Related Changes in Plasma Extracellular Vesicle Characteristics and Internalization by Leukocytes. Sci Rep *7*.

Feldman, N., Rotter-Maskowitz, A., and Okun, E. (2015). DAMPs as mediators of sterile inflammation in aging-related pathologies. Ageing Res. Rev. *24*, 29–39.

Franceschi, C., and Campisi, J. (2014). Chronic inflammation (inflammaging) and its potential contribution to age-associated diseases. J. Gerontol. A Biol. Sci. Med. Sci. *69 Suppl 1*, S4-9.

Fucikova, J., Moserova, I., Urbanova, L., Bezu, L., Kepp, O., Cremer, I., Salek, C., Strnad, P., Kroemer, G., Galluzzi, L., et al. (2015). Prognostic and Predictive Value of DAMPs and DAMP-Associated Processes in Cancer. Front Immunol *6*.

Garg, A.D., Galluzzi, L., Apetoh, L., Baert, T., Birge, R.B., Bravo-San Pedro, J.M., Breckpot, K., Brough, D., Chaurio, R., Cirone, M., et al. (2015). Molecular and Translational Classifications of DAMPs in Immunogenic Cell Death. Front Immunol *6*.

Gillet, L.C., Navarro, P., Tate, S., Röst, H., Selevsek, N., Reiter, L., Bonner, R., and Aebersold, R. (2012). Targeted data extraction of the MS/MS spectra generated by data-independent acquisition: a new concept for consistent and accurate proteome analysis. Mol. Cell Proteomics *11*, O111.016717.

Hernandez-Segura, A., de Jong, T.V., Melov, S., Guryev, V., Campisi, J., and Demaria, M. (2017). Unmasking Transcriptional Heterogeneity in Senescent Cells. Curr. Biol. *27*, 2652-2660.e4.

Hernandez-Vallejo, S.J., Beaupere, C., Larghero, J., Capeau, J., and Lagathu, C. (2013). HIV protease inhibitors induce senescence and alter osteoblastic potential of human bone marrow mesenchymal stem cells: beneficial effect of pravastatin. Aging Cell *12*, 955–965.

Ho, J.E., Mahajan, A., Chen, M.-H., Larson, M.G., McCabe, E.L., Ghorbani, A., Cheng, S., Johnson, A.D., Lindgren, C.M., Kempf, T., et al. (2012). Clinical and genetic correlates of growth differentiation factor 15 in the community. Clin. Chem. *58*, 1582–1591.

Ho, J.E., Hwang, S.-J., Wollert, K.C., Larson, M.G., Cheng, S., Kempf, T., Vasan, R.S., Januzzi, J.L., Wang, T.J., and Fox, C.S. (2013). Biomarkers Of Cardiovascular Stress And Incident Chronic Kidney Disease. Clin Chem *59*, 1613–1620.

Huang, J., Xie, Y., Sun, X., Zeh, H.J., Kang, R., Lotze, M.T., and Tang, D. (2015). DAMPs, Ageing, and Cancer: The 'DAMP Hypothesis.' Ageing Res Rev *24*, 3–16.

Jeon, O.H., David, N., Campisi, J., and Elisseeff, J.H. (2018). Senescent cells and osteoarthritis: a painful connection. J. Clin. Invest. *128*, 1229–1237.

Kaur, G., and Levy, E. (2012). Cystatin C in Alzheimer's disease. Front Mol Neurosci *5*.

Keerthikumar, S., Chisanga, D., Ariyaratne, D., Al Saffar, H., Anand, S., Zhao, K., Samuel, M., Pathan, M., Jois, M., Chilamkurti, N., et al. (2016). ExoCarta: A Web-Based Compendium of Exosomal Cargo. Journal of Molecular Biology *428*, 688–692.

Kuilman, T., Michaloglou, C., Vredeveld, L.C.W., Douma, S., van Doorn, R., Desmet, C.J., Aarden, L.A., Mooi, W.J., and Peeper, D.S. (2008). Oncogene-induced senescence relayed by an interleukin-dependent inflammatory network. Cell *133*, 1019–1031.

Nelson, G., Wordsworth, J., Wang, C., Jurk, D., Lawless, C., Martin-Ruiz, C., and von Zglinicki, T. (2012). A senescent cell bystander effect: senescence-induced senescence. Aging Cell *11*, 345–349.

Neuwirth, E. (2014). RColorBrewer: ColorBrewer Palettes.

Neves, J., Demaria, M., Campisi, J., and Jasper, H. (2015). Of flies, mice, and men: evolutionarily conserved tissue damage responses and aging. Dev Cell *32*, 9–18.

O'Brien, R.J., and Wong, P.C. (2011). Amyloid Precursor Protein Processing and Alzheimer's Disease. Annu Rev Neurosci *34*, 185–204.

Ohkouchi, S., Ono, M., Kobayashi, M., Hirano, T., Tojo, Y., Hisata, S., Ichinose, M., Irokawa, T., Ogawa, H., and Kurosawa, H. (2015). Myriad Functions of Stanniocalcin-1 (STC1) Cover Multiple Therapeutic Targets in the Complicated Pathogenesis of Idiopathic Pulmonary Fibrosis (IPF). Clin Med Insights Circ Respir Pulm Med *9*, 91–96.

Özcan, S., Alessio, N., Acar, M.B., Mert, E., Omerli, F., Peluso, G., and Galderisi, U. (2016). Unbiased analysis of senescence associated secretory phenotype (SASP) to identify common components following different genotoxic stresses. Aging (Albany NY) *8*, 1316–1327.

Pan, J.S.-C., Huang, L., Belousova, T., Lu, L., Yang, Y., Reddel, R., Chang, A., Ju, H., DiMattia, G., Tong, Q., et al. (2015). Stanniocalcin-1 Inhibits Renal Ischemia/Reperfusion Injury via an AMP-Activated Protein Kinase-Dependent Pathway. J Am Soc Nephrol *26*, 364–378.

Pedregosa, F., Varoquaux, G., Gramfort, A., Michel, V., Thirion, B., Grisel, O., Blondel, M., Prettenhofer, P., Weiss, R., Dubourg, V., et al. (2011). Scikit-learn: Machine Learning in Python. Journal of Machine Learning Research *12*, 2825−2830.

Rardin, M.J., Schilling, B., Cheng, L.Y., MacLean, B.X., Sorensen, D.J., Sahu, A.K., MacCoss, M.J., Vitek, O., and Gibson, B.W. (2015). MS1 Peptide Ion Intensity Chromatograms in MS2 (SWATH) Data Independent Acquisitions. Improving Post Acquisition Analysis of Proteomic Experiments. Mol Cell Proteomics *14*, 2405–2419.

Rodier, F., Coppé, J.P., Patil, C.K., Hoeijmakers, W.A., Muñoz, D.P., Raza, S.R., Freund, A., Campeau, E., Davalos, A.R., and Campisi, J. (2009). Persistent DNA damage signalling triggers senescence-associated inflammatory cytokine secretion. Nat Cell Biol *11*, 973–979.

Rohatgi, A., Patel, P., Das, S.R., Ayers, C.R., Khera, A., Martinez-Rumayor, A., Berry, J.D., McGuire, D.K., and de Lemos, J.A. (2012). Association of growth differentiation factor-15 with coronary atherosclerosis and mortality in a young, multiethnic population: observations from the Dallas Heart Study. Clin. Chem. *58*, 172–182.

Rosas, I.O., Richards, T.J., Konishi, K., Zhang, Y., Gibson, K., Lokshin, A.E., Lindell, K.O., Cisneros, J., MacDonald, S.D., Pardo, A., et al. (2008). MMP1 and MMP7 as Potential Peripheral Blood Biomarkers in Idiopathic Pulmonary Fibrosis. PLoS Med *5*.

Rosenberger, G., Koh, C.C., Guo, T., Röst, H.L., Kouvonen, P., Collins, B.C., Heusel, M., Liu, Y., Caron, E., Vichalkovski, A., et al. (2014). A repository of assays to quantify 10,000 human proteins by SWATH-MS. Sci Data *1*, 140031.

Roy, R., Yang, J., and Moses, M.A. (2009). Matrix Metalloproteinases As Novel Biomarkers and Potential Therapeutic Targets in Human Cancer. J Clin Oncol *27*, 5287–5297.

Schilling, B., Gibson, B.W., and Hunter, C.L. (2017). Generation of High-Quality SWATH® Acquisition Data for Label-free Quantitative Proteomics Studies Using TripleTOF® Mass Spectrometers. Methods Mol Biol *1550*, 223–233.

Shahim, P., Blennow, K., Johansson, P., Svensson, J., Lista, S., Hampel, H., Andersson, L.C., and Zetterberg, H. (2017). Cerebrospinal Fluid Stanniocalcin-1 as a Biomarker for Alzheimer's Disease and Other Neurodegenerative Disorders. Neuromolecular Med. *19*, 154–160.

Shannon, P., Markiel, A., Ozier, O., Baliga, N.S., Wang, J.T., Ramage, D., Amin, N., Schwikowski, B., and Ideker, T. (2003). Cytoscape: a software environment for integrated models of biomolecular interaction networks. Genome Res. *13*, 2498–2504.

Sharma, V., Eckels, J., Taylor, G.K., Shulman, N.J., Stergachis, A.B., Joyner, S.A., Yan, P., Whiteaker, J.R., Halusa, G.N., Schilling, B., et al. (2014). Panorama: A Targeted Proteomics Knowledge Base. J Proteome Res *13*, 4205–4210.

Sharma, V., Eckels, J., Schilling, B., Ludwig, C., Jaffe, J.D., MacCoss, M.J., and MacLean, B. (2018). Panorama Public: A Public Repository for Quantitative Data Sets Processed in Skyline. Mol. Cell Proteomics *17*, 1239–1244.

Su, J., Guo, B., Zhang, T., Wang, K., Li, X., and Liang, G. (2015). Stanniocalcin-1, a new biomarker of glioma progression, is associated with prognosis of patients. Tumour Biol. *36*, 6333–6339.

Takasugi, M. (2018). Emerging roles of extracellular vesicles in cellular senescence and aging. Aging Cell *17*.

Tanaka, T., Biancotto, A., Moaddel, R., Moore, A.Z., Gonzalez-Freire, M., Aon, M.A., Candia, J., Zhang, P., Cheung, F., Fantoni, G., et al. (2018). Plasma proteomic signature of age in healthy humans. Aging Cell *17*, e12799.

Tchkonia, T., Zhu, Y., van Deursen, J., Campisi, J., and Kirkland, J.L. (2013). Cellular senescence and the senescent secretory phenotype: therapeutic opportunities. J Clin Invest *123*, 966–972.

Théry, C., Amigorena, S., Raposo, G., and Clayton, A. (2006). Isolation and characterization of exosomes from cell culture supernatants and biological fluids. Curr Protoc Cell Biol *Chapter 3*, Unit 3.22.

Tominaga, K. (2015). The emerging role of senescent cells in tissue homeostasis and pathophysiology. Pathobiol Aging Age Relat Dis *5*.

Valentijn, F.A., Falke, L.L., Nguyen, T.Q., and Goldschmeding, R. (2018). Cellular senescence in the aging and diseased kidney. J Cell Commun Signal *12*, 69–82.

Wallentin, L., Zethelius, B., Berglund, L., Eggers, K.M., Lind, L., Lindahl, B., Wollert, K.C., and Siegbahn, A. (2013). GDF-15 for prognostication of cardiovascular and cancer morbidity and mortality in men. PLoS ONE *8*, e78797.

Warnes, G.R., Bolker, B., Bonebakker, L., Gentleman, R., Liaw, W.H.A., Lumley, T., Maechler, M., Magnusson, A., Moeller, S., Schwartz, M., et al. (2019). gplots: Various R Programming Tools for Plotting Data.

Wollert, K.C., Kempf, T., and Wallentin, L. (2017). Growth Differentiation Factor 15 as a Biomarker in Cardiovascular Disease. Clinical Chemistry *63*, 140–151.